Gravin regulates centrosome function through PLK1

Erica G. Colicino[1], Alice M. Garrastegui[1, 4], Judy Freshour[1], Peu Santra[1], Dawn E. Post[2], Leszek Kotula[2, 3], Heidi Hehnly[1, 2]

[1]Department of Cell and Developmental Biology, Upstate Medical University
750 E. Adams Street Syracuse, NY 13202

[2]Department of Urology, Upstate Medical University
750 E. Adams Street Syracuse, NY 13202

[3]Department of Biochemistry, Upstate Medical University
750 E. Adams Street Syracuse, NY 13202

[4]Department of Biology, Syracuse University
900 South Crouse Ave. Syracuse, NY 13244

Keywords: PLK1, Gravin, CEP215, centrosome, micronuclei

ABSTRACT

Here we propose to understand how the mitotic kinase PLK1 drives chromosome segregation errors, with a specific focus on Gravin, a PLK1 scaffold. In both 3-D primary prostate cancer cell cultures that are prone to Gravin-depletion and Gravin shRNA treated cells, an increase in cells containing micronuclei was noted when compared to controls. To examine whether the loss of Gravin affected PLK1 distribution and activity we utilized photokinetics and a PLK1 activity-biosensor. Gravin-depletion resulted in an increased PLK1 mobile fraction, causing the redistribution of active-PLK1 that leads to increased defocusing and phosphorylation of the mitotic centrosome protein CEP215 at serine-613. Gravin-depletion further led to defects in microtubule re-nucleation from mitotic centrosomes, decreased kinetochore-fiber integrity, increased incidence of chromosome misalignment, and subsequent micronuclei formation following mitosis completion. Murine Gravin rescued chromosome misalignment and micronuclei formation, but a mutant Gravin that cannot bind PLK1 did not. These findings suggest that disruption of a Gravin–PLK1 interface leads to inappropriate PLK1 activity contributing to chromosome segregation errors, micronuclei formation, and subsequent DNA-damage.

INTRODUCTION

The focus of this study is to understand the spatial regulation of the mitotic kinase, Polo-like kinase 1 (PLK1), during mitosis. This question remains enigmatic due to a multiplicity of PLK1 interactions and substrates located at distinct subcellular sites. Here we examine a PLK1 scaffold protein, Gravin/AKAP12/SSeCKS, that localizes to pericentriolar material (PCM) and cytosol (Gelman, 2010; Hehnly *et al.*, 2015). Gravin has been defined as a scaffold for several kinases (Gelman, 2010). Canton et al demonstrated *in vitro* that PLK1 interacts with Gravin through a phosphorylated threonine at 766 (Canton *et al.*, 2012), which validated an earlier proteomics screen that identified Gravin as a possible PLK1 scaffold (Lowery *et al.*, 2007). Gravin-depletion was then shown to cause a prometaphase delay and chromosome instability through FISH-analysis of chromosome 18 (Canton *et al.*, 2012). Gravin also interacts with Aurora A kinase, arguing that Gravin, similarly to CEP192 (Joukov *et al.*, 2014) and Bora (Chan *et al.*, 2008), has the potential to facilitate a mitotic signaling cascade between Aurora A and PLK1 (Hehnly *et al.*, 2015). The direct interactions and localization patterns of Gravin and PLK1 were previously characterized (Canton *et al.*, 2012; Hehnly *et al.*, 2015). However, these studies did not thoroughly examine or definitively determine how, in live cells, Gravin regulates PLK1 distribution, activity, or downstream function, which is the main focus of this study.

PLK1 misregulation can drive chromosome missegregation and subsequent micronuclei formation (Lera and Burkard, 2012). Abnormal mitotic kinase expression and activity, such as with PLK1, has been linked to genomic instability in prostate cancer (Deeraksa *et al.*, 2013). Microarray-based studies demonstrated a 3- to 10-fold reduction in relative Gravin mRNA levels in breast, prostate, lung, ovarian, testicular, and other cancer types compared to controls (Gelman, 2010). One plausible mechanism to generate substantial local mutagenesis observed in prostate cancer is by physically isolating one or two chromosomes and partitioning them into micronuclei. Chromosomes in micronuclei can be subject to massive DNA damage (Holland and Cleveland, 2012). Here we are testing the hypothesis that Gravin-loss inappropriately distributes PLK1 signaling during mitosis driving chromosome missegregation leading to micronuclei formation.

RESULTS AND DISCUSSION

Gravin-loss is associated with increased micronuclei formation in primary prostate cancer cells.

We first analyzed primary hormone therapy-resistant prostate epithelial cells in 3-dimensional (3-D) cultures (derived from (Gao *et al.*, 2014)) in parallel with an immortalized prostate epithelial cell line, RWPE-1. Using this system we found that Gravin can be significantly down-regulated in primary prostate cancer cells. By comparing two primary patient samples PCa1 and PCa3 to an immortalized prostate epithelial cell line RWPE-1 or to a control primary prostate epithelial cell line 26Na, we found that Gravin expression is diminished in PCa1 (Figure 1A). When 3-D primary cultures (Figure 1A-E) and prostate epithelial cells genetically modified using Gravin shRNA (Figure 1F-H) were compared, an increase in mitotic delay or micronuclei formation was noted in cells that lacked Gravin. Micronuclei are structures formed as a

result of lagging chromosomes that contain either whole or partial chromosomes outside of the macronucleus (Crasta *et al.*, 2012). Specifically, PCa1 cells that display a significant reduction in Gravin expression (Figure 1A) had an increase in mitotic index compared to both control and PCa3 cells (Figure 1B, D). PCa1 also contained 25.04 ± 2.35% of cells containing micronuclei compared to 2.65 ± 1.10% in control and 10.43 ± 3.93% in PCa3 (Figure 1C, E). These results suggest that Gravin-loss contributes to micronuclei formation found in PCa1. From this, we wanted to know if the effects of Gravin-loss on micronuclei formation are the result of inappropriate PLK1 distribution and/or activity causing chromosome missegregation.

Gravin-loss disrupts PLK1 dynamics predominately at mitotic centrosomes.

It is unclear how the loss of Gravin impacts PLK1 in live cells during mitosis. One possibility is that scaffold proteins, such as Gravin, help coordinate the appropriate spatial organization of PLK1 to direct the flow of molecular information. Previous studies identified that Gravin phosphorylation at T766 primes it for PLK1 binding (modeled in Figure 2A) and this interaction takes place, at least in part, at mitotic centrosomes (Canton *et al.*, 2012; Hehnly *et al.*, 2015). However, these studies did not examine how this interaction regulates the spatial and temporal dynamics of PLK1 in live cells. By structured illumination microscopy (SIM) we confirmed our previous studies (Hehnly *et al.*, 2015) that Gravin localizes to mitotic centrosomes (Figure 2B, a', orange arrow) along with PLK1 (Figure 2B, b', orange arrows). Additionally, PLK1 localizes to kinetochores (Figure 2B, b', magenta arrow) and later in mitosis at the cytokinetic midbody (Figure 2C). Due to the similar localization patterns between Gravin and PLK1 at mitotic centrosomes we predict that Gravin-loss may disrupt PLK1 dynamics at this locale in live cells during mitosis.

We first examined whether there was a difference in PLK1 dynamics between the mitotic centrosomes, kinetochores, and cytokinetic midbody. A previous study carefully compared the Fluorescence Recovery After Photobleaching (FRAP) kinetics of PLK1 at each of these locales by overexpression of GFP-PLK1 and analysis at 30°C in a human osteosarcoma cell line, U2OS (Kishi *et al.*, 2009). Instead of transiently expressing PLK1, we utilized a cell line with normal ploidy expressing a PLK1 shRNA to eliminate endogenous PLK1 and exogenously expressed an shRNA resistant GFP-PLK1 at endogenous levels (RPE cells, Figure 2C). In addition, FRAP analysis was performed at 37°C. Similar to the previous study (Kishi *et al.*, 2009), we found significantly different dynamics between mitotic centrosomes, kinetochores, and the cytokinetic midbody for GFP-PLK1 (Figure 2C-D, Supplementary Figure 1A). However, the half-life of PLK1 at each of these locales was considerably shorter than what was reported in (Kishi *et al.*, 2009), (Figure 2D). We predict this is the case due to endogenous expression levels of PLK1 and 37°C incubation.

We next compared GFP-PLK1 dynamics in Gravin-depleted RPE cells (Gravin shRNA) to control RPE cells (control shRNA; Supplementary Figure 1B). Gravin-depleted cells had a significant decrease in GFP-PLK1 half-life at kinetochores (Figure 2E, Supplementary Figure 1C-D) and mitotic centrosomes (Figure 2E, H) and no significant difference at cytokinetic midbodies (Supplementary Figure 1F-G). We then compared the immobile fraction of GFP-PLK1 at each locale, i.e. the fraction of GFP-PLK1 that remains after photobleaching. Gravin-depleted cells demonstrated a 12%

decrease in the immobile fraction at mitotic centrosomes when compared to controls (Figure 2E, I). However, no difference in the immobile fraction was observed at kinetochores or at the cytokinetic midbody (Figure 2E, Supplementary Figure 1E, H).

Using control and Gravin-depleted cells rescued ectopically with wild-type Gravin or Gravin (T766A) that cannot bind PLK1 (Canton *et al.*, 2012), we repeated the FRAP experiments at individual mitotic centrosomes (Figure 2F-G, expression levels following rescues in Supplementary Figure 1B). A significant proportion of GFP-PLK1 fluorescence was not recovered at mitotic centrosomes in control shRNA and Gravin-rescued cells, representing the immobile fraction of PLK1. In Gravin-depleted and Gravin (T766A) rescue cells GFP-PLK1 fluorescence is almost fully recovered 3 seconds post bleach (Figure 2F-G). After analysis of multiple metaphase cells, rescue with Gravin (T766A) caused a significant decrease in the immobile fraction and in the half-life of GFP-PLK1 when compared to wild-type Gravin rescue (Figure 2H, I). With wild-type Gravin rescue there is a slight increase in total Gravin expression compared to controls, which is likely causing the significant increase in the immobile fraction of GFP-PLK1 (42.68% immobile) compared to control shRNA (25.33% immobile, Figure 2H). Collectively, these findings suggest that GFP-PLK1 dynamics at mitotic centrosomes is partly regulated by its binding scaffold Gravin.

Gravin-depleted cells redistribute active-PLK1 causing increased phosphorylation events at mitotic centrosomes.

We utilized a fluorescence resonance energy transfer (FRET)-based phosphorylation sensor (Macůrek *et al.*, 2008) to test whether Gravin-loss causes a change in PLK1 activity. The PLK1-biosensor is composed of a monomeric CFP and YFP flanking a PLK1 specific c-jun substrate sequence tethered by a flexible linker to an FHA2 phospho-threonine binding domain (Liu *et al.*, 2012). The phosphorylation of the PLK1 substrate triggers an intramolecular clamp with the FHA2 causing a conformational change, decreasing the amount of FRET from CFP to YFP (Figure 3A). The FRET-biosensor provides a fluorometric readout for PLK1 phosphorylation and a decrease in FRET is measured upon increased activity of PLK1. For ease of interpretation, we plotted an inverse ratio of YFP excitation to YFP emission over CFP excitation to YFP emission (Figure 3B) so that an increase in the inverse FRET ratio represents an increase in PLK1 activity. To determine whether anchoring of PLK1 by Gravin affected PLK1's activity, we either monitored the PLK1 biosensor in cycling cells (Supplementary Figure 2A-B) or cells synchronously released from mitotic arrest by nocodazole (Figure 3C-D, Supplementary Figure 2C). For these studies we utilized HEK293 cells treated with either a control shRNA or Gravin shRNA with or without addition of the PLK1 inhibitor, BI2536. In control cells treated with BI2536 a significant decrease in the inverse FRET ratio was calculated (Supplementary Figure 2C), suggesting that our FRET ratio was accurately measuring PLK1 activity. In cells depleted of Gravin, a significant increase in the inverse FRET ratio was calculated when compared to control cells (median of 1.703 compared to 3.09 for Gravin depleted cells, Figure 3C-D), and the increase was lost after treatment with the PLK1 inhibitor BI2536 indicating that the increase requires PLK1 kinase activity (median of 1.63, Figure 3C-D). Previous studies reported that an upstream PLK1 kinase, Aurora A, activates PLK1 during mitosis by phosphorylating it at T210, binds to Gravin (Macůrek *et al.*, 2008). We

confirmed that Gravin-loss resulted in a modest decrease in T210 phosphorylation ((Hehnly *et al.*, 2015), Supplementary Figure 2D-E). However, Gravin-loss caused a significant increase in the FRET-biosensor fluorometric readout (Figure 3C-D). One possibility is that Gravin-depleted cells display a slight decrease in global PLK1 activity, shown by decreased phosphorylated at T210, however a population of active-PLK1 is redistributed in cells, allowing for increased phosphorylation and unregulated access towards its substrates. Thus, we conclude that we are not causing an increase in overall activity of PLK1, but a change in distribution of already active PLK1 with Gravin-loss.

Since Gravin and PLK1 likely interact on mitotic centrosomes (Figure 2B, E, (Hehnly *et al.*, 2015)), we tested for changes in PLK1 centrosome substrate phosphorylation with loss of Gravin. To mimic the localization of possible endogenous PLK1 centrosome substrates, we attached a pericentrin-AKAP450-centrosomal-targeting domain (PACT) to the c-terminus of the FRET biosensor (FRET-PACT), which successfully targets the PLK1 biosensor to mitotic centrosomes (Figure 3E). To examine FRET-PACT response to changes in PLK1 activity in living cells, we imaged mitotic HEK293 cells treated with a control shRNA, Gravin shRNA, and/or the PLK1 inhibitor, BI2536. As with the cytosolic PLK1 FRET biosensor, the centrosome-targeted biosensor demonstrated a significant increase in the inverse FRET ratio in Gravin-depleted cells (median of 2.83) compared to control (median of 2.13, Figure 3F). Treatment with BI2536 decreased the FRET ratio for both control cells (median of 1.84) and for Gravin-depleted cells (median of 2.18, Figure 3F).

We confirmed the increase in phosphorylation seen with the FRET-PACT biosensor by isolating mitotic centrosomes (Hung *et al.*, 2015) from control and Gravin depleted cells. Gravin-depleted mitotic centrosomes displayed a significant increase in phospho-Serine/phospho-Threonine (pS/pT) compared to controls (Figure 3G, H). We next examined a putative centrosome-localized PLK1 substrate, CEP215 (Santamaria *et al.*, 2011), for increased phosphorylation in Gravin-depleted cells compared to control (Figure 3I). Immunoblot analysis detected a 3-fold increase in PLK1-dependent pS/pT levels in FLAG-CEP215 isolated from Gravin shRNA treated cell lysate compared to control lysate or lysates treated with BI2536 (Figure 3I-K). A previous phosphoproteomics screen of PLK1 substrates identified a PLK1 phosphorylation site on CEP215 at its serine-613 residue (Santamaria *et al.*, 2011). Through sequence alignment we found that this serine is conserved between human and murine CEP215 (Supplementary Figure 2F). We immunoprecipitated a FLAG-tagged non-phosphorylatable mutant CEP215 (S613A) or wild-type FLAG-CEP215, and FLAG-CEP215-S613A presented with decreased pS/pT phosphorylation compared to FLAG-CEP215 (Figure 3L-M), suggesting that serine-613 is phosphorylated. Collectively, these data support the idea that Gravin constrains a subset of PLK1 to be released at the right time and place. When Gravin is depleted, this subset of PLK1 is now free to inappropriately phosphorylate downstream substrates, one of which is CEP215 at serine 613 (modeled in Figure 3N).

Gravin-loss results in CEP215 disorganization and disrupted mitotic centrosome function.

Since CEP215 phosphorylation is increased in Gravin-depleted cells, we examined if its organization at the mitotic centrosomes were affected in HEK293 cells

treated with Gravin shRNA. Using stimulated emission depletion microscopy (STED), CEP215 in control cells clustered into a ring-like structure at both mitotic centrosomes (Figure 4A). In Gravin-depleted cells we found that CEP215 no longer organized symmetrically across the two poles. One pole contained more CEP215 that was no longer organized in a ring and the other pole contained diffusely arranged CEP215. Line scans across multiple cells that bisect the mitotic centrosomes demonstrated a specific decrease in CEP215 organization on one pole over the other in Gravin depleted cells compared to controls (Figure 4A). We then measured the fluorescence intensity of CEP215 at mitotic centrosomes in cells treated with either control or Gravin shRNA. Gravin-depleted cells contained significantly less CEP215 at mitotic centrosomes compared to controls (Figure 4B). When calculating the ratio of the mitotic centrosome with the highest CEP215 fluorescence intensity over the mitotic centrosome with the lowest, Gravin-depleted cells presented with a significantly greater ratio (Figure 4C). Together, this data suggests that Gravin-loss causes decreased CEP215 organization and localization at mitotic centrosomes, leading to an asymmetric distribution of CEP215 between the two mitotic centrosomes.

To determine whether Gravin-loss, and subsequent CEP215 disorganization and distribution, leads to defects in centrosome function, we performed a functional test to monitor mitotic centrosome-mediated MT-nucleating activity over time in HEK293 cells. Spindles were disassembled with nocodazole, and examined at different times after nocodazole washout for MT nucleation. At 0 min there was less tubulin at mitotic centrosomes in Gravin-depleted cells than controls. At 2 min of regrowth, mitotic centrosomes in control cells showed an increased ability to nucleate MTs (Figure 4D-E). This activity was modestly impaired at first in Gravin-depleted cells, but by 5 min both Gravin-depleted cells and control cells were nucleating MTs to a similar degree, and by 20 min Gravin-depleted cells formed a complete spindle whereas control cells were still recovering from the regrowth (Figure 4D). This finding suggests that the initial defects in nucleation at 0 and 2 min could be caused by downstream defects in PLK1 target organization, such as CEP215 which is known to organize the γ-tubulin ring complex (Fong *et al.*, 2008). Following this, the redistribution of active-PLK1 caused by Gravin-loss likely contributes to the rapid increase in nucleation and spindle assembly after nocodazole washout (Figure 4D-E). One possible consequence to defects in centrosome function and/or abnormal PLK1 activity is a loss in kinetochore fiber integrity (Paschal *et al.*, 2012; Hehnly and Doxsey, 2014). To test if Gravin-loss affects kinetochore fiber integrity, we employed cold treatment to specifically eliminate dynamic microtubules from mitotic HEK293 cells. Kinetochore fibers in control cells were well organized and robust (Figure 4F). Following Gravin depletion, kinetochore fibers were completely lost in 31 ± 3.84% of mitotic cells (Figure 4G). A previous study reported that an active form of PLK1, PLK1 T210D, resulted in labile kinetochore fibers when compared to wild-type control (Paschal *et al.*, 2012). This finding, in combination with our findings, suggests that redistribution of active-PLK1 caused by Gravin-loss disrupts centrosome function and kinetochore fiber integrity.

Gravin loss and increased phosphorylation of CEP215 results in higher incidence of cells containing micronuclei.

PLK1 is an essential kinase in the regulation of mitotic progression by allowing the passage of cells through the G2/M cell cycle checkpoints (Zitouni *et al.*, 2014). Premature passage of these checkpoints through overactive PLK1 has been shown to cause genomic instability in cells through lagging chromosomes and DNA damage (Pan *et al.*, 2009). In addition, a disruption in centrosome function, through the loss of centrioles, also results in increased lagging chromosomes and micronuclei formation (Sir *et al.*, 2013). Thus, we examined if Gravin-depleted cells, which have decreased centrosome function (Figure 4D-E), present with lagging chromosomes. Comparing 3-D prostate epithelial cells depleted of Gravin to control, we noted an increase in lagging chromosomes (Supplementary Figure 3A). To monitor this quantitatively in live cells, we utilized a GFP-H2B HeLa cell line stably depleted of Gravin (Gravin shRNA, Supplementary Figure 3B-D) compared to controls, where only 42.28 ± 11.20% of Gravin-depleted cells displayed normal chromosome alignment compared to 81.16 ± 6.90% of control cells. Of the remaining cells, 32.37 ± 6.17% of dividing Gravin-depleted cells presented with lagging chromosomes compared to 7.95 ± 3.44% in control cells (Supplementary Figure 3B-C). These findings suggest that Gravin-loss contributes to increased chromosome segregation defects. We further tested whether lagging chromosomes can be rescued in cells when Gravin is re-introduced (Figure 5A-B, Supplementary Figure 3D). We found that cells lacking Gravin or expressing Gravin T766A contained lagging chromosomes compared to rescue cells with wild-type Gravin suggesting that the binding of Gravin to PLK1 is essential for proper chromosome alignment during metaphase.

Since chromosome misalignment can result in micronuclei formation (Crasta *et al.*, 2012), we examined whether disrupting the Gravin-PLK1 interface resulted in increased micronuclei formation. In Gravin-depleted cells we found that 22.87 ± 3.92% of cells formed micronuclei, whereas rescue with full-length wild-type Gravin lead to a significant reduction in micronuclei formation (down to 9.3 ± 2.88%, Figure 5C-D). When Gravin-depleted cells were rescued with Gravin-T766A, 32.03 ± 5.61% of cells displayed micronuclei formation. To confirm that loss of Gravin resulted in increased micronuclei formation we compared wild-type and Gravin-null MEFs (Supplementary Figure 3E-F). Gravin-null MEFs resulted in a 2-fold increase in micronuclei formation compared to controls (Supplementary Figure 3F). This data suggests that disruption of the Gravin-PLK1 interface results in lagging chromosomes and micronuclei formation (modeled in Fig 5K). Previous studies suggested that micronuclei form from lagging chromosomes develop DNA breaks (Leibowitz *et al.*, 2015). Since disrupting the Gravin-PLK1 binding interaction causes an increase in chromosome mis-segregation and micronuclei formation (Figure 5A-D), we examined if these micronuclei had an increased incidence in developing DNA breaks by staining for γ-H2AX (Figure 5C, E). Of cells rescued with Gravin-T766A that contained micronuclei, 76.37 ± 24.66% contained γ-H2AX-positive micronuclei compared to 33.33 ± 11.55% of wild-type Gravin rescue cells (Figure 5E).

CEP215 phosphorylation by PLK1 at serine-613 when Gravin is depleted (Fig 3I-M) results in CEP215 disorganization at mitotic centrosomes (Figure 4A-C). Thus, we tested in Gravin-depleted cells whether CEP215-S613A can alleviate chromosome missegregation errors and micronuclei formation compared to a phospho-mimetic mutant CEP215-S613E or wild-type CEP215 (Figure 5F-J, Supplementary Figure 3G).

The FLAG-tagged non-phosphorylatable mutant (S613A) and the FLAG-tagged phosphomimetic mutants (S613E) localize to mitotic spindle poles in control and Gravin-depleted cells (Supplementary Figure 3G) and to the interphase centrosome in Gravin-depleted cells (Figure 5H). We found that 73.33 ± 4.81% of cells expressing FLAG-CEP215 and 70.67 ± 3.53% of cells expressing FLAG-CEP215-S613E presented with lagging chromosomes compared to 42.67 ± 9.62% in cells expressing FLAG-CEP215-S613A (Figure 5I). The percentage of cells expressing FLAG-CEP215 (47 ± 2.65%) or FLAG-CEP215-S613E (48.33 ± 2.19%) contained significantly more micronuclei compared to cells expressing FLAG-CEP215-S613A (24.67 ± 0.67%, Figure 5J). This data suggests that the PLK1-dependent CEP215 phosphorylation at S613 leads to increased chromosome instability through the formation of lagging chromosomes and micronuclei formation. Together, our findings suggest that blocking the ability of Gravin to scaffold PLK1 causes an increase in DNA damage (Figure 5K). This is a potential mechanism for how chromosome-instability can arise upon PLK1 deregulation in prostate cancer.

MATERIALS AND METHODS

Cell culture: 3-D RWPE human prostate epithelial cells were grown in Keratinocyte SFM combo from Life Technologies/Fisher (cat 17-005-042) with 60% Matrigel (Fisher cat no CB40234C; Corning no 356237). 2-D PLK1-GFP RPE, GFP-H2B HeLa (Hehnly and Doxsey, 2014), mouse embryonic fibroblasts (MEFs) isolated from wild type and Gravin null mice, and human embryonic kidney (HEK) 293ad cells were grown in 1X Dulbecco's Modified Eagle Medium (DMEM, Gibco™) supplemented with 10% Seradigm FBS (VWR) and 1% penicillin-streptomycin (10,000U/ml) (Gibco™). Phoenix-AMPHO cells were used for viral-production in Gravin rescue experiments, grown in 1X Dulbecco's Modified Eagle Medium (DMEM, Gibco™) supplemented with 10% FBS (Sigma) and 1% penicillin-streptomycin (10,000U/ml) (Gibco™). All cultures are maintained at 37°C with 5% CO_2.

Human primary prostate cancer epithelial cells (PCa1, PCa3) were grown as 3-D-organoid cultures (Gao *et al.*, 2014). Cells were plated in 200μl DMEM/F12 media containing supplements in a multi-well plate (Ibidi cell chambers #80827, PCa1 and PCa3 at 3000 cells/well) coated with collagen type II. Media supplements included EGF, R-spondin 1, noggin, FGF10, FGF2, dihydrotestosterone (DHT), nicotinamide, the TGF-b/Alk inhibitor A83-01, the p38 MAK kinase inhibitor SB202190, the ROCK inhibitor Y-27632, B27 additive, N-Acetyl-L-cysteine, glutamax, HEPES, and primocin. Following seeding, media was removed and cells overlaid with 200μl of 50% GFR (growth factor reduced) matrigel (GFR-matrigel from Fisher cat no CB40230C; Corning no 356231) and 50% mixture.

shRNA and FRET constructs: Cells depleted of Gravin were made using a lentivirus-infected shRNA specific to Gravin (AKAP12 (Gravin) shRNA sc-40305-v). Control cells were treated with a control shRNA (sc-108080). Gravin rescue experiments were performed using the wild-type and phospho-dead mutant T766A of the murine Gravin (SSECKS) gene. FRET experiments were performed using a PLK1 FRET biosensor containing a PLK1 specific c-jun substrate (Liu *et al.*, 2012). In order to examine PLK1 activity specifically at mitotic centrosomes, a localized PLK1 FRET-biosensor was constructed by fusing the above FRET biosensor to the PACT domain (human pericentrin-kendrin) using a 10 amino acid linker (R-A-Q-A-S-N-S-G-R-P) as done for kinetochores in (Liu *et al.*, 2012). All constructs verified through sequencing.

Antibodies and chemical inhibitors: For western blot analysis and immunofluorescence imaging, the following antibodies were used: phospho-Histone H3 (Ser10) 1:200, Cell Signaling 9701S), mouse anti-PLK1 (E-2) (1:250, Santa Cruz sc-55504) (1:200), rabbit anti-PLK1 (1:100, Cell signaling #4513S), mouse anti-Centrin (1:1,000, EMD Millipore 04-1624), mouse anti-Gravin (1:250, Sigma Aldrich 45-G3795), anti-α tubulin conjugated with FITC (1:250, Sigma Aldrich F2168), Actinred 555vReady Probes reagent (Thermo Fisher Scientific R37112), NucBlue Fixed Cell Stain from Ready Probes (Thermo Fisher Scientific R37606), rabbit anti-γ-histone H2A.X (Ser 139, γ-H2AX) (1:500, Cell Signaling 9718S), anti-CEP215 (1:500, Bethyl Laboratories IHC-00063), anti-acetylated tubulin (1:500, Sigma 45-T6793), and phospho-Serine/Threonine (1:40, Fisher Scientific 01-672-764). Horseradish peroxidase (HRP)

conjugated antibodies included: donkey anti-mouse IgG (H+L) (Jackson ImmunoResearch Labs 715-035-150), donkey anti-rabbit IgG (H+L) (Jackson ImmunoResearch Labs 711-035-152), and mouse anti-GAPDH (1:10,000, Sigma Aldrich 45-G9295). Fluorescent secondary antibodies include: AlexaFluor donkey anti-mouse 488 (Life Technologies A21202), 568 (Life Technologies A10037), and 647 (Life Technologies A31571), AlexaFluor donkey anti-rabbit 488 (Life Technologies A21206), 568 (Life Technologies A10042), 647 (Life Technologies A31573).

Immunofluorescence for 3-D cultures/2-D cultures: Using a pipette, as in (Hung *et al.*, 2016), media was carefully removed from cultures. Cultures were rinsed with PBS and fixed with 4% paraformaldehyde (PFA) at room temperature for 30 minutes with light shaking. The PFA was carefully removed and replaced with fresh PFA for an additional 30 minutes with light shaking. After the PFA was removed, 50mM NH_4Cl was added for 10 minutes. Cells were washed with PBS for 30 minutes, with light shaking, and then treated for 5 minutes with 0.1% Triton-X, blocked with PBSΔT (PBS, 1% BSA, 0.5% Triton X-100), and incubated with primary antibodies for 4 hrs at room temperature. Cultures were washed 3xs with PBSΔT and incubated with secondary antibodies for 4 hours at room temperature. Cultures were kept in PBS containing DABCO (1,4-Diazabicyclo[2.2.2]octane) antifade reagent (200mM) for imaging.

Cells were plated on #1.5 coverslips until they reached 90% confluence, and fixed using methanol (-20°C). Cells were rehydrated in PBS before blocking in PBSΔT for 30 minutes. Primary antibodies diluted in PBSΔT were added to coverslips and incubated for 1 hour at room temperature, followed by 10 washes with PBSΔT, secondary antibodies for 1 hour at room temperature, and then 10 washes with PBSΔT. Coverslips were rinsed with diH_2O and mounted on glass slides using Prolong Diamond with DAPI mounting media.

Imaging: Cells were imaged using either a Leica DMi8 STP800 (Leica, Bannockburn, IL) equipped with a Lumencor SPECTRA X (Lumencor, Beaverton, Or) with a Hamamatsu ORCAflash 4.0 V2 CMOS C11440-22CU camera using either a 40×1.15 N.A. Lamda S LWD objective or 100×/1.4 N.A. HC PI Apo oil emersion objective and Metamorph software to acquire images or a PerkinElmer (Waltham, MA) Ultraview VoX Spinning Disc Confocal system on a Nikon Eclipse Ti-E microscope using a Hammamatsu C9100-50 EMCCD camera and a 100×/1.4 N.A. Apo oil emersion objective using Volocity software. Super-resolution 3D-SIM images were acquired on a DeltaVision OMX V4 (GE Healthcare) equipped with a 60×/1.42 NA PlanApo oil immersion lens (Olympus), 405-, 488-, 568-, and 642-nm solid-state lasers and sCMOS cameras (pco.edge). Image stacks of 5–6 µm with 0.125-µm thick z-sections and 15 images per optical slice (3 angles and 5 phases) were acquired using immersion oil with a refractive index 1.518. Images were reconstructed using Wiener filter settings of 0.003 and optical transfer functions measured specifically for each channel with SoftWoRx 6.1.3 (GE Healthcare). Images from different color channels were registered using parameters generated from a gold grid registration slide (GE Healthcare) and SoftWoRx 6.1.3 (GE Healthcare). STED imaging was performed using a Leica TCS SP8 (Leica, Bannockburn, IL) equipped with STED 3X, a super-continuum laser (white light laser 470-670nm) for excitation, 592/546/600nm STED depletion lasers, and HCS PL APO

100x/1.40 oil STED white objective. Images were acquired using the Leica LAS software and post-image processing of STED images was performed using SVI Huygens deconvolution software.

FRAP experiments were performed using a Leica SP5 scanning confocal microscope (Leica, Bannockburn, IL) with an HCX Plan Apochromat 63×/1.40-0.06 NA OIL objective or the PerkinElmer (Waltham, MA) Ultraview VoX Spinning Disc Confocal system on a Nikon Eclipse Ti-E microscope. With the Leica SP5 the LAS AF (Leica Application Suite Advanced Fluorescence) software (Leica) FRAP wizard was used to acquire images. The ImageJ FRAP Calculator Macro plug-in was used to generate FRAP curves and generate half-life and immobile fraction values. Graphs were then produced in Prism GraphPad software.

Fluorescence Resonance Energy Transfer (FRET): HEK293ad cells were transfected with a PLK1 FRET or a PLK1 FRET-PACT sensor using Mirus Bio TransIT-LT1 transfection reagent (Hukasova *et al.*, 2012; Liu *et al.*, 2012; Bruinsma *et al.*, 2015). After 24 hours cells were synced for 8 hours using 100nM nocodazole and released. To inhibit PLK1 cells were treated with 100nM BI2536 for 20 minutes. Images were acquired on a Leica DMi8 STP800 (Leica, Bannockburn, IL) using a 63×/1.4 N.A. HC PI Apo oil emersion objective. The $YFP^{ex} \rightarrow YFP^{em}/CFP^{ex} \rightarrow YFP^{em}$ emission ratio in each image was calculated after background subtraction and averaged over multiple cells. FRET ratio was calculated using ImageJ Ratio-Plus plugin. Experiments were repeated multiple times with similar results.

Mitotic Centrosome Isolation: HEK 293ad cells were treated with 100nM nocodazole for 18hours. A mitotic shake-off was then performed and centrosome isolation as described in (Hung *et al.*, 2015). In short, HEK293ad cells were treated with 20 μg/ml cytochalasin D and 10 μg/ml nocodazole for 2 hours. Cells were then washed with the following buffers in order: 1X PBS, 0.1%PBS:8% w/w sucrose, 8% w/w sucrose, LB (1mM Tris-HCL, 8 mM BME). Cells were then treated with 1ml (per 100mm plate) LB+0.5% NP40 containing phosphatase inhibitors at 4°C for 2 minutes on rocker. Supernatants were collected and centrifuged at 1500 g for 6 minutes at 4°C. The supernatants were then transferred to tubes containing 5 mls Ficoll (20% diluted in PE buffer (10mM PIPES, 1mM EDTA, 8mM BME)), centrifuged at 13,000 g for 15 minutes at 4°C, and the Ficoll-PE interface (~150μl) was collected. The interface was diluted in PE buffer containing phosphatase inhibitors and isolated onto coverslips by centrifugation. Mitotic centrosomes were fixed with ice-cold methanol and immunostained for pS/pT and centrin.

Immunoprecipitation: HEK293ad cells were transfected with 5μg (per 100mm plate) FLAG-CEP215. After 48 hours, cells were lysed using ice-cold HEPES lysis buffer (25mM HEPES, 150mM NaCl, 0.5% Tritonx100, 1mM EDTA, 1mM EGTA, 2% Glycerol, 10mM NaF) then incubated on ice for 10 minutes, and post-nuclear supernatant collected. 600μg-1mg protein was incubated with anti-FLAG M2 affinity gel beads (Sigma) for 1.5 hours at 4°C on rotator. Beads were washed 2x with lysis buffer and isolated beads were boiled in 30uL sample buffer before western blot analysis.

Ice treatment: HEK293ad cells treated with either control shRNA or Gravin shRNA were placed in Leibovitz's L-15 media (ThermoFisher #21083027) and placed on ice for 5 minutes. After 5 minutes the cells were washed in PBS and fixed in ice-cold methanol at -20°C for 10 minutes. Cells were then immunolabeled and imaged for analysis.

Microtubule Re-nucleation Assay: HEK293ad cells were treated with 10μg nocodazole in media for 1 hour. Cells were then washed 3-times with PBS before being placed in media at 37°C for times indicated. Cells were fixed using ice-cold methanol at -20°C, immunolabeled, and imaged for analysis.

Image Analysis: 0.2 μm Z-steps of cell volumes are presented as maximum projections using ImageJ. AutoQuant deconvolution was used on wide-field images using Metamorph software. Integrated intensities were measured on sum projections as described in (Hoffman *et al.*, 1995). To measure integrated intensity on either isolated centrosomes or mitotic centrosomes circular regions of interest (ROIs) were drawn. The larger ROI (ROI^L) is used to measure background where the center smaller ROI (ROI^S) measures signal. The following equation was used: integrated intensity of ROI^L -((integrated intensity of ROI^S –integrated intensity of ROI^L)*(area ROI^L /(area ROI^S -area ROI^L))) (Hehnly and Doxsey, 2014). Line scans were performed by calculating the normalized fluorescence intensity across a single line. Graphs and statistical analysis (unpaired-student t-tests or ANOVA analysis as labeled) were completed using Graphpad Prism software. Error bars represent ± SEM, $p < 0.05$ were considered to be statistically significant. All images were set to a resolution of 300 DPI or greater after image analysis from raw data.

ACKNOWLEDGEMENTS
The work was supported by the National Institutes of Health grant R00GM107355 (to H.H.), the Department of Defense grant PC160083 (to H.H.), the Carol Baldwin Foundation of Central N.Y. (to H.H.), R01 CA161018 (to L.K.), and the Department of Health Prostate Cancer Hypothesis Development RFA #1410200115 (to L.K. and H.H.). We thank René Medema for providing us with the PLK1-FRET biosensor plasmid, Patrina Pellett (previously at G.E., currently at Oxford Nanoimaging) for assistance obtaining SIM images, and Geoff Daniels and Jessica Shivas (Leica) for assistance obtaining STED images. We thank Wenyi Feng (Upstate) and Jeff Amack (Upstate) for critical feedback.

AUTHOR CONTRIBUTIONS
E.C., P.S., A.G., and H.H. designed and conducted experiments and analyzed the data under the supervision of H.H.. J.F. constructed all viral vectors. D.P. maintained primary prostate cancer cell lines and is under the supervision of L.K. Technical expertise was provided by L.K. and D.P.. E.C. and H.H. wrote the manuscript. All authors critically read and contributed to the manuscript.

CONFLICT OF INTEREST
The authors declare that they have no conflict of interest.

REFERENCES

Bruinsma, W., Aprelia, M., Kool, J., Macurek, L., Lindqvist, A., and Medema, R. H. (2015). Spatial Separation of Plk1 Phosphorylation and Activity. Front. Oncol. *5*, 1–8.

Canton, D. A., Keene, C. D., Swinney, K., Langeberg, L. K., Nguyen, V., Pelletier, L., Pawson, T., Wordeman, L., Stella, N., and Scott, J. D. (2012). Gravin Is a Transitory Effector of Polo-like Kinase 1 during Cell Division. Mol. Cell *48*, 547–559.

Chan, E. H. Y., Santamaria, A., Silljé, H. H. W., and Nigg, E. A. (2008). Plk1 regulates mitotic Aurora A function through betaTrCP-dependent degradation of hBora. Chromosoma *117*, 457–469.

Crasta, K., Ganem, N. J., Dagher, R., Lantermann, A. B., Ivanova, E. V, Pan, Y., Nezi, L., Protopopov, A., Chowdhury, D., and Pellman, D. (2012). DNA breaks and chromosome pulverization from errors in mitosis. Nature *482*, 53–58.

Deeraksa, A., Pan, J., Sha, Y., Liu, X.-D., Eissa, N., Lin, S.-H., and Yu-Lee, L.-Y. (2013). Plk1 is upregulated in androgen-insensitive prostate cancer cells and its inhibition leads to necroptosis. Oncogene *32309*, 2973–2983.

Fong, K.-W., Choi, Y.-K., Rattner, J. B., and Qi, R. Z. (2008). CDK5RAP2 Is a Pericentriolar Protein That Functions in Centrosomal Attachment of the γ-Tubulin Ring Complex. Mol. Biol. Cell *19*, 115–125.

Gao, D. *et al.* (2014). Organoid cultures derived from patients with advanced prostate cancer. Cell *159*, 176–187.

Gelman, I. H. (2010). Emerging Roles for SSeCKS/Gravin/AKAP12 in the Control of Cell Proliferation, Cancer Malignancy, and Barriergenesis. Genes Cancer *1*, 1147–1156.

Hehnly, H., Canton, D., Bucko, P., Langeberg, L. K., Ogier, L., Gelman, I., Santana, L. F., Wordeman, L., and Scott, J. D. (2015). A mitotic kinase scaffold depleted in testicular seminomas impacts spindle orientation in germ line stem cells. Elife *4*, e09384.

Hehnly, H., and Doxsey, S. (2014). Rab11 Endosomes Contribute to Mitotic Spindle Organization and Orientation. Dev. Cell *28*, 497–507.

Hoffman, D. B., Pearson, C. G., Yen, T. J., Howell, B. J., and Salmon, E. D. (1995). Microtubule-dependent Changes in Assembly of Microtubule Motor Proteins and Mitotic Spindle Checkpoint Proteins at PtK1 Kinetochores. Mol. Biol. Cell *12*.

Holland, A. J., and Cleveland, D. W. (2012). Chromoanagenesis and cancer: mechanisms and consequences of localized, complex chromosomal rearrangements. Nat. Med. *18*, 1630–1638.

Hukasova, E., Silva Cascales, H., Kumar, S. R., and Lindqvist, A. (2012). Monitoring Kinase and Phosphatase Activities Through the Cell Cycle by Ratiometric FRET. J. Vis. Exp., e3410–e3410.

Hung, H.-F., Hehnly, H., and Doxsey, S. (2015). Methods to analyze novel liaisons between endosomes and centrosomes. Biophys. Methods Cell Biol. *130*, 47–58.

Hung, H. F., Hehnly, H., and Doxsey, S. (2016). The mother centriole appendage protein cenexin modulates lumen formation through spindle orientation. Curr. Biol. *26*, 793–801.

Joukov, V., Walter, J. C., and De Nicolo, A. (2014). The Cep192-Organized Aurora A-Plk1 Cascade Is Essential for Centrosome Cycle and Bipolar Spindle Assembly. Mol. Cell *55*, 578–591.

Kishi, K., van Vugt, M. a T. M., Okamoto, K., Hayashi, Y., and Yaffe, M. B. (2009). Functional dynamics of Polo-like kinase 1 at the centrosome. Mol. Cell. Biol. *29*, 3134–3150.

Leibowitz, M. L., Zhang, C.-Z., and Pellman, D. (2015). Chromothripsis: A New Mechanism for Rapid Karyotype Evolution. Annu. Rev. Genet. *49*, 183–211.

Lera, R. F., and Burkard, M. E. (2012). High Mitotic Activity of Polo-like Kinase 1 Is Required for Chromosome Segregation and Genomic Integrity in Human Epithelial Cells. J. Biol. Chem. *287*, 42812–42825.

Liu, D., Davydenko, O., and Lampson, M. A. (2012). Polo-like kinase-1 regulates kinetochore-microtubule dynamics and spindle checkpoint silencing. J. Cell Biol. *198*, 491–499.

Lowery, D. M., Clauser, K. R., Hjerrild, M., Lim, D., Alexander, J., Kishi, K., Ong, S.-E., Gammeltoft, S., Carr, S. A., and Yaffe, M. B. (2007). Proteomic screen defines the Polo-box domain interactome and identifies Rock2 as a Plk1 substrate. EMBO J. *26*, 2262–2273.

Macůrek, L., Lindqvist, A., Lim, D., Lampson, M. a, Klompmaker, R., Freire, R., Clouin, C., Taylor, S. S., Yaffe, M. B., and Medema, R. H. (2008). Polo-like kinase-1 is activated by aurora A to promote checkpoint recovery. Nature *455*, 119–123.

Pan, S.-H., Tai, C.-C., Lin, C.-S., Hsu, W.-B., Chou, S.-F., Lai, C.-C., Chen, J.-Y., Tien, H.-F., Lee, F.-Y., and Wang, W.-B. (2009). Epstein-Barr virus nuclear antigen 2 disrupts mitotic checkpoint and causes chromosomal instability. Carcinogenesis *30*, 366–375.

Paschal, C. R., Maciejowski, J., and Jallepalli, P. V (2012). A stringent requirement for Plk1 T210 phosphorylation during K-fiber assembly and chromosome congression. Chromosoma *121*, 565–572.

Santamaria, A., Wang, B., Elowe, S., Malik, R., Zhang, F., Bauer, M., Schmidt, A., Silljé, H. H. W., Körner, R., and Nigg, E. a (2011). The Plk1-dependent phosphoproteome of the early mitotic spindle. Mol. Cell. Proteomics *10*, M110.004457.

Sir, J. H., Pütz, M., Daly, O., Morrison, C. G., Dunning, M., Kilmartin, J. V., and Gergely, F. (2013). Loss of centrioles causes chromosomal instability in vertebrate somatic cells. J. Cell Biol. *203*, 747–756.

Zitouni, S., Nabais, C., Jana, S. C., Guerrero, A., and Bettencourt-Dias, M. (2014). Polo-like kinases: structural variations lead to multiple functions. Nat Rev Mol Cell Biol *15*, 433–452.

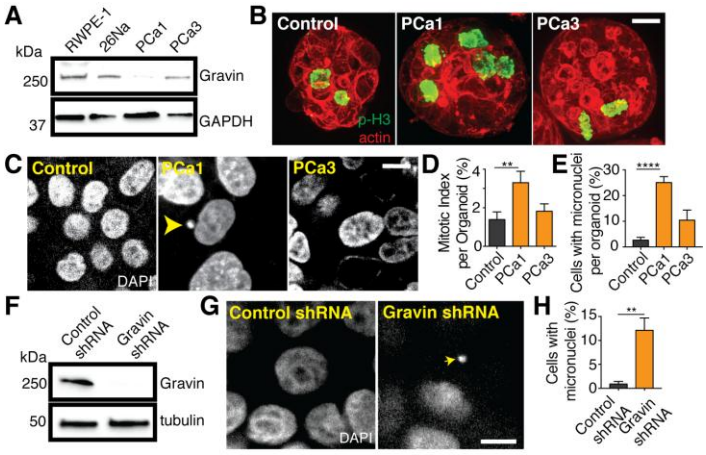

Figure 1. Gravin-loss is associated with increased micronuclei formation in primary prostate cancer cells.

(A) Immunoblot analysis showing decreased Gravin expression in PCa1 and PCa3 cancer cells compared to RWPE-1 and normal patient prostate epithelium cells (26Na). (B) Control (RWPE-1), PCa1, and PCa3 3-D acini cultures fluorescently labeled for p-H3 (green) and actin (red). (C) Control (RWPE-1), PCa1, and PCa3 3-D acini labeled for DAPI (grey) displaying micronuclei within a single cell (yellow arrowhead). Confocal micrographs for (B,C) are presented as maximum projections. Bar, 5μm. (D, E) Quantification of the mitotic index (D) and cells (%) with micronuclei (E) for control (RWPE), PCa1, and PCa3 in 3-D acini was calculated. (n=30 organoids over n=3 experiments ±SEM, Student's t-test $p = 0.0099$ (D) and Student's t-test $p < 0.0001$ (E)). (F) Immunoblot analysis of Gravin expression in RWPE-1 cells expressing a control GAPDH shRNA or a Gravin shRNA. Tubulin was used as loading control. (G) Control shRNA and Gravin shRNA RWPE-1 3-D acini cultures stained for DAPI displaying micronuclei within a single cell (yellow arrow). Bar, 5μm. (H) Quantification of Gravin shRNA and control shRNA treated cells with micronuclei (%) over n=3 experiments ±SEM (Student's t-test $p = 0.0097$).

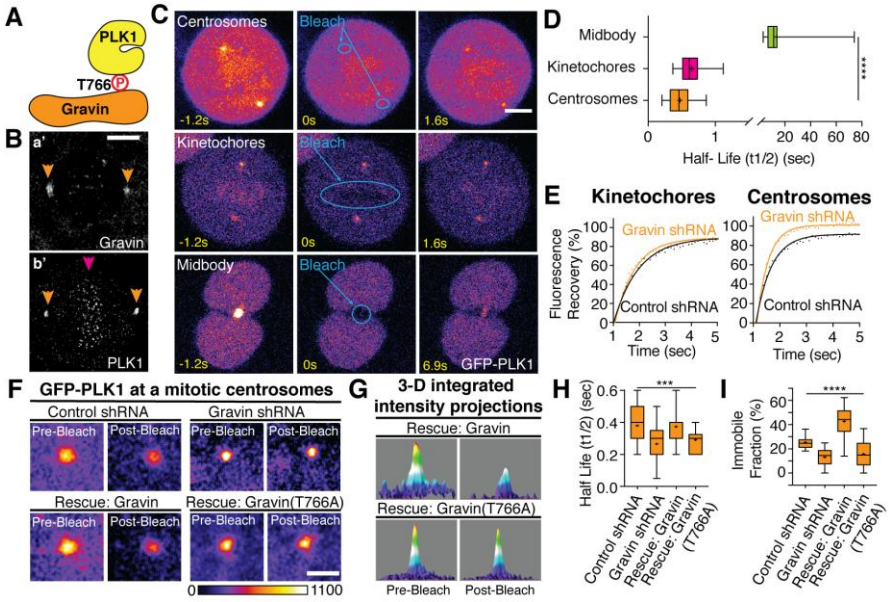

Figure 2. Gravin loss disrupts PLK1 dynamics predominately at mitotic centrosomes.

(A) Model depicting Gravin (orange) binding PLK1 (yellow) at phosphorylated T766, (Canton et al. 2012). (B) Maximum projection of structured illumination microscopy (SIM) micrographs of Gravin (a') and PLK1 (b') localizing to mitotic centrosomes (orange arrows) in metaphase cells. (magenta arrow represents PLK1 localization at kinetochores in b'). (C) Representative images of Fluorescence Recovery After Photobleaching (FRAP) of GFP-PLK1 (Fire LUT, ImageJ) RPE cells at mitotic centrosomes, kinetochores, and cytokinetic midbody. Bar, 5μm. (D) Quantification presented as box-and-whisker plot of half-life for GFP-PLK1 in control and Gravin-shRNA treated cells (+ indicates mean, n > 20 cells across n = 3 experiments, ANOVA analysis indicates significance of $p<0.0001$). (E) A curve was fit using one-phase decay of PLK1 fluorescence recovery at kinetochores (left) and mitotic centrosomes (right) in metaphase cells treated with control or Gravin shRNAs, (n>20cells over n=3 experiments). (F) GFP-PLK1 at a single metaphase mitotic centrosome in control shRNA or Gravin shRNA treated cells rescued with full-length wild-type Gravin, or T766A mutant Gravin prior to and 3 seconds after bleaching events. Confocal micrographs at a single mitotic centrosome are shown (Fire LUT, Image J, bar indicates gradient of integrated fluorescent intensity values (A.U.)). Bar, 2μm. (G) Integrated intensity profiles for GFP-PLK1 at a single mitotic centrosome before and 3 seconds after bleaching events are presented. (H,I) The average (H) Half-life (t1/2) and (I) immobile fraction of GFP-PLK1 at metaphase spindle poles was calculated and presented as box-and-whisker plots with + indicating mean (n>20 cells over n=3 experiments, One-way ANOVA analysis indicates significance between conditions of $p<0.001$ for (H), and $p<0.0001$ for (I)).

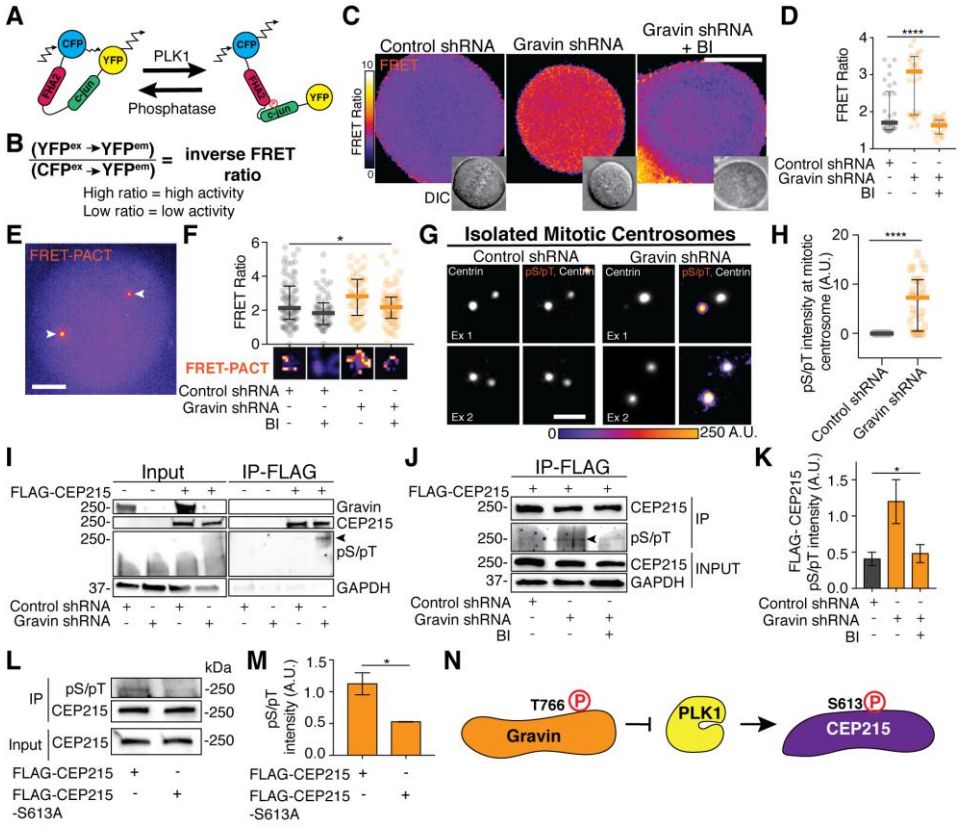

Figure 3. Gravin-depleted cells redistribute active-PLK1 causing increased phosphorylation events at mitotic centrosomes.

(A) Model of PLK1-biosensor showing how increased PLK1 activity causes a conformational change in the biosensor through phosphorylation of c-jun (green) and binding of the FHA2 domain (magenta), resulting in a loss of FRET. When there is increased phosphatase activity, the PLK1-biosensor is in a relaxed state, allowing FRET. (B) Equation for determining the inverse FRET ratio by dividing the $YFP^{EX} \rightarrow YFP^{EM}$ by the $CFP^{EX} \rightarrow YFP^{EM}$. By calculating the inverse FRET ratio, high ratios correspond with high levels of PLK1 activity while low ratios correspond to low levels of PLK1 activity. (C) Relative PLK1 activity shown as an inverse FRET ratio (Fire LUT, ImageJ, bar indicates gradient of FRET ratio values) and DIC images taken from nocodazole synchronized and released cells in metaphase. Control shRNA, Gravin shRNA, and Gravin shRNA cells plus BI2536 are shown. Bar, 5μm. (D) Quantification of the inverse FRET-efficiency nocodazole released cells in metaphase that were treated with control shRNA, Gravin shRNAs, and/or BI2536 (BI) is presented as a scatter plot (n>30 cells over n=3 experiments, median with interquartile range shown, One-way ANOVA p<0.0001). (E) PLK1-FRET-PACT biosensor localization in metaphase cells.

Arrows depict mitotic centrosomes, (Fire LUT). Bar, 5μm. (F) The inverse FRET-efficiency of the PLK1-FRET-PACT probe was quantified from nocodazole synchronized and released metaphase cells treated with control shRNA, Gravin shRNA, and/or BI2536 (BI), and presented as a scatter plot. Representative single mitotic centrosome inverse FRET ratios shown below graph (FIRE-LUT). (n>50 cells over n=4 experiments, median with interquartile range shown, One-way ANOVA p=0.0371). (G) Isolated mitotic centrosomes from control shRNA and Gravin shRNA HEK293 cells immunolabeled for centrin (white) and pSerine/pThreonine (pS/pT) (FIRE LUT). Bar, 2μm. (H) Quantification of pS/pT intentsity at mitotic centrosomes in (G) presented as a scatter plot (n=27 centrioles for each treatment, median with interquartile range shown, Student's t-test p<0.0001). (I-J) FLAG IP of Mock or FLAG-CEP215 transfected control shRNA or Gravin shRNA ± BI2536 treated HEK293 cells as indicated. Protein expression and immunoprecipitation was analyzed by immunoblot for Gravin, CEP215, pS/pT, and GAPDH (as loading control). Black arrowhead indicates pS/pT band at 250 kDa. (K) Quantification of pS/pT intensities normalized over total FLAG-CEP215 IP, (n=3 experiments ±SEM, One-way ANOVA p=0.0353). (L) Immunoblot analysis of FLAG-CEP215 and FLAG-CEP215-S613A IP from HEK293 cells. (M) Quantification of pS/pT expression levels from FLAG-IP normalized over total FLAG-CEP215 (n=3 experiments ±SEM, Student's t-test p=0.0264). (N) Working model depicting that phosphorylated Gravin (orange) inhibits PLK1 (yellow) from phosphorylating CEP215 (purple) during mitosis.

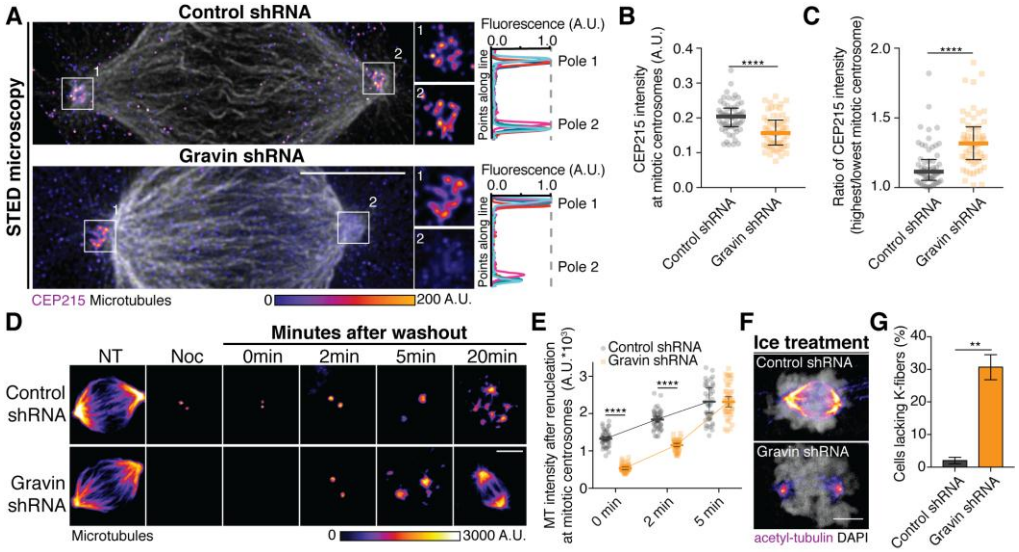

Figure 4. Gravin-loss results in CEP215 disorganization and disrupted mitotic centrosome function.

(A) STED (stimulated emission-depletion) micrographs of metaphase control and Gravin shRNA HEK293 cells are presented as maximum projections. Cells were immunostained for CEP215 (Fire-LUT, ImageJ, bar indicates gradient of integrated fluorescent intensity values (A.U.)) and tubulin (white). Bar, 5μm. Inserts (white boxes) depict 2x magnification of CEP215 at mitotic centrosomes. A line scan through the mitotic centrosomes is drawn and the normalized fluorescence intensity of CEP215 is plotted (right, each line represents a single line scan over n=5 cells for each treatment). (B) Quantification of total CEP215 fluorescence intensity at mitotic centrosomes in control and Gravin shRNA treated HEK293ad cells (n=3 experiments, n=60 cells, median with interquartile range shown, Student's t-test, $p<0.0001$). (C) Ratio of highest CEP215 intensity over lowest CEP215 intensity between the two mitotic centrosomes within a single cell (n=60 cells over n=3 experiments, median with interquartile range shown, Student's t-test $p<0.0001$). (D) A series of confocal micrographs demonstrating MT regrowth (α-tubulin, Fire-LUT, bar indicates gradient of integrated fluorescent intensity values (A.U.)) at mitotic centrosomes for a time course following nocodazole washout in HEK293 cells treated with Gravin or control shRNAs. Micrographs presented as maximum projections. Bar, 5μm. (E) The integrated α-tubulin intensity at mitotic centrosomes was quantified and presented as a scatter plot at indicated times following washout (n = 50 poles for each time and treatment, median with interquartile range shown, representative of n = 3 experiments, Student's t-test for 0 min ($p < 0.0001$), 2 min ($p < 0.0001$), 5 min ($p = 0.60$)). (F) Maximum confocal projections of control shRNA and Gravin shRNA mitotic HEK293 cells treated for 5 minutes on ice. Cells were immunostained for acetylated-tubulin (Fire-LUT, ImageJ) and DAPI (white). (G) Quantification of cells (%) lacking K-fibers in HEK293 cells treated with control or Gravin shRNAs calculated over n=3 experiments ± SEM (Student's t-test $p=0.0020$).

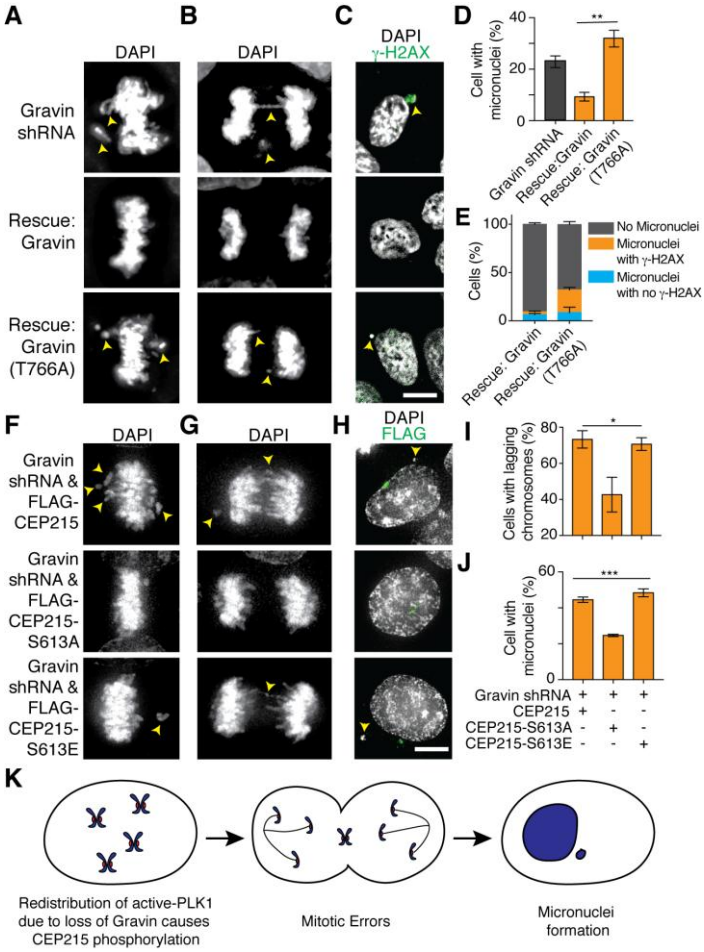

Figure 5. Gravin loss and increased phosphorylation of CEP215 results in higher incidence of cells containing micronuclei.

(A-C) Wide-field deconvolved micrographs of Gravin shRNA, full-length Gravin rescue, and mutant T766A Gravin cells are presented as maximum projections. Cells were immunostained for DAPI (A, B, C white) and γ-H2AX (C, green). Bar, 5μm. (D) Quantification of cells containing micronuclei (%) in Gravin shRNA treated cells rescued with full-length Gravin or Gravin (T766A) over n=3 experiments ±SEM, Student's t-test p-value=0.0034. (E) Quantification of cells containing micronuclei with γH2AX (%) in Gravin shRNA cells rescued with full-length Gravin or Gravin (T766A) over n=3 experiments ± SEM. (F-H) Deconvolved wide-field micrographs of Gravin shRNA treated cells expressing FLAG-CEP215, FLAG-CEP215-S613A, or FLAG-CEP215-S613E presented as maximum projections. Cells were immunolabeled for DAPI (F, G, H, white) and FLAG (H, green). Bar, 5μm. (I, J) Quantification of cells containing lagging

chromosomes (I) and micronuclei (J) (%) in Gravin shRNA cells expressing FLAG-CEP215, FLAG-CEP215-S613A, or FLAG-CEP215-S613E (n=3 experiments ±SEM, n>300cells, One-way ANOVA p=0.0290 (I), p=0.0003 (J)). (K) Model summarizing that when Gravin is lost, a redistribution of active-PLK1 leads to mitotic errors and subsequent micronuclei formation.